Geophys. J. Int. (1991) **106**, 537–550

Source parameters of large earthquakes in the East Anatolian Fault Zone (Turkey)

Tuncay Taymaz,[1] Haluk Eyidoğan[2] and James Jackson[1]

[1] *Department of Earth Sciences, Bullard Laboratories, Madingley Rise, Madingley Road, Cambridge* CB3 0EZ, *UK*
[2] *İTÜ Maden Fakültesi, Jeofizik Bölümü, Maslak* 80626, *İstanbul, Turkey*

Accepted 1991 March 14. Received 1991 March 12; in original form 1990 September 27

SUMMARY

The East Anatolian Fault Zone accommodates most of the motion between the Arabian plate and the apparently little-deforming interior of central Turkey. The direction of overall slip across this zone is crucial to the determination of the slip rate on the North Anatolian Fault. We use long-period *P*- and *SH*-waveforms to determine the source parameters of the four largest earthquakes that occurred in, or near, the East Anatolian Fault Zone in the last 35 years. Only one of these actually involved left-lateral strike–slip motion on a NE–SW fault. But the other three, and the nearby 1975 Lice earthquake, all had steeply dipping nodal planes with a NNW strike: if these were the auxiliary planes then all the earthquakes had a slip vector direction within about 10° of 063°. If this direction represents the Arabia–Turkey motion, then the slip rate on the North Anatolian Fault must be in the range 31 to 48 mm yr^{-1}, with a probable value of 38 mm yr^{-1}, and the overall slip rate across the East Anatolian Fault Zone must be about 29 mm yr^{-1} with a range of 25–35 mm yr^{-1}.

Key words: continental tectonics, earthquakes, East Anatolia, faulting, Turkey.

1 INTRODUCTION

The East Anatolian Fault Zone (EAFZ) is a band of active seismicity and tectonism that joins the eastern end of the North Anatolian Fault Zone to the Mediterranean Sea in the Gulf of İskenderun (see inset to Fig. 1). It is much less distinct, both morphologically and structurally, than the North Anatolian Fault, which ruptured almost along its entire length in a series of large earthquakes between 1939 and 1967 (Ambraseys 1970). There has been little seismicity associated with the East Anatolian Fault Zone this century, though many large earthquakes are known to have occurred in or near it within the last 500 years (Ambraseys 1971, 1989: see also Fig. 11 and Table 3). Although some clear strands of NE–SW left-lateral strike–slip faulting are visible on satellite images (McKenzie 1976), the structure of the zone is more complicated than this (Fig. 1): with several pull-apart basins, conjugate fractures, and also considerable thrusting and folding (Arpat & Şaroğlu 1972; Perinçek 1979; Dewey *et al.* 1986; Perinçek, Günay & Kozlu 1987; Lybéris *et al.* 1990). Structures within the zone are rarely continuous for longer than a few tens of km, and discontinuities between fault segments may have controlled the extent of rupture in historical earthquakes (Barka & Kadinsky-Cade 1988).

A knowledge of the motions in the East Anatolian Fault Zone is crucial for an understanding of the present-day kinematics of the eastern Mediterranean. East of the junction between the North and East Anatolian Fault Zones (near Karlıova, Fig. 1) is a region of mixed strike–slip and thrust faulting that extends from the Turkey–Iraq border north into the Caucasus (Jackson & McKenzie 1984; Philip *et al.* 1989). This region accommodates the shortening between Arabia and Eurasia, which began about 12 Myr ago (Şengör, Görür & Şargoğlu 1985; Dewey *et al.* 1986) and which is proceeding today at a rate of about 27 mm yr^{-1} in a direction 335°, based on the NUVEL-1 plate motion model of DeMets *et al.* (1990). Central Turkey is a relatively flat, elevated plateau, and although it is neither completely aseismic (Jackson & McKenzie 1984), nor devoid of active faults (Şengör *et al.* 1985; Perinçek *et al.* 1987), its morphology and seismicity suggest that it is relatively inactive compared with the North and East Anatolian Fault Zones. For this reason, McKenzie (1972) and Jackson & McKenzie (1984) thought that most of the Eurasia–Turkey motion was accommodated on the North Anatolian Fault Zone, and most of the Arabia–Turkey motion was taken up on the East Anatolian Fault Zone. The slip vectors in earthquakes on the North Anatolia Fault Zone define a pole of rotation between Turkey and Eurasia near 14.6°N 34.0°E

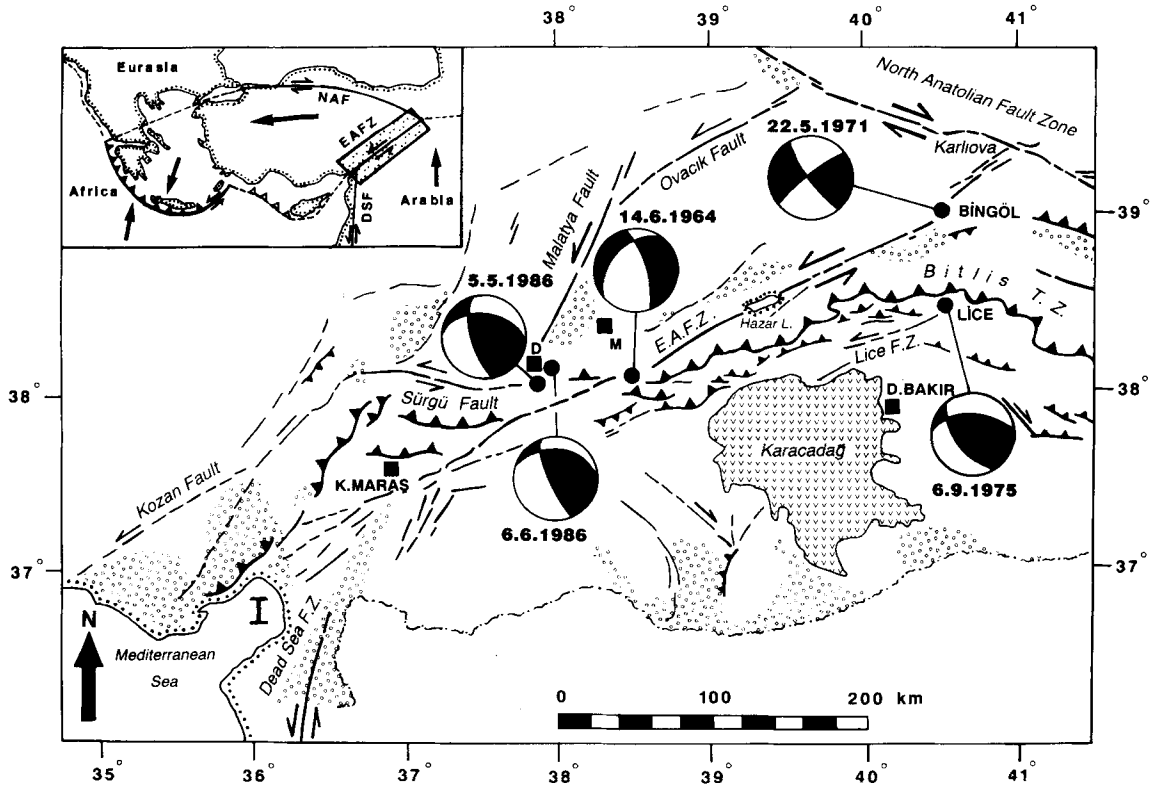

Figure 1. Summary map of the EAFZ, compiled from our observations and those of Şengör *et al.* (1985), Dewey *et al.* (1986), Perinçek *et al.* (1987) and Perinçek & Çemen (1990). Lower hemisphere projections of the focal mechanisms corresponding to the minimum misfit solutions of the earthquakes studied by us and by Nábělek (1984) are shown. Compressional quadrants are shaded. Dates identify the events in Table 1. This map shows the major structural features in the East Anatolian Fault Zone and its Arabian Foreland showing fractures (fine lines), mapped faults (thick lines), Plio-Quaternary, Quaternary basins (dotted areas) and major volcanic fields (marked as Karacadağ). D = Doğanşehir; M = Malatya; I = Gulf of İskenderun. Inset shows the motions of the Arabian and African plates, central Turkey, and the southern Aegean Sea, relative to Europe. The dashed line in the north Aegean is not a plate boundary: it joins the end of the North Anatolian Fault (NAF) to the northern end of the Hellenic Trench (shown as a thrust), and emphasizes that the westward motion of Turkey is accommodated partly by convergence along the west and southwest coast of Greece and Albania (see Taymaz *et al.* 1991). EAFZ: East Anatolian Fault Zone (the stippled area); DSF: Dead Sea Fault.

(Jackson & McKenzie 1984). By assuming that the motion on the East Anatolian Fault Zone was in the direction 060°, parallel to the strike of the obviously active strike–slip faults within the East Anatolian Fault Zone, McKenzie (1972) and Jackson & McKenzie (1984) were able to estimate the magnitude of the velocities on both the North and East Anatolian Fault Zones. This logic is illustrated at the end of the paper, in Fig. 12, which shows the velocity triangle between the Eurasian, Arabian and Turkish plates near Karlıova. The direction and length (or magnitude) of one side (Arabia–Eurasia) is known (from NUVEL-1). The direction, but not the length, of another side (Turkey–Eurasia) is known from the slip vectors on the North Anatolian Fault. By fixing the slip vector between Arabia and Turkey (i.e. the direction of the third side), the triangle is complete, and the lengths and directions of all sides are known. The magnitude of the velocity on the North Anatolian Fault is a powerful influence on the tectonics of the Aegean region farther west (Jackson & McKenzie 1988a, b; Taymaz, Jackson & McKenzie 1991). Because the slip vector direction across the East Anatolian Fault Zone is so central to quantitative descriptions of the kinematics in the eastern Mediterranean, we were anxious to re-examine the evidence for it, and to further constrain its orientation using the source parameters of moderate-sized earthquakes.

Since the installation of the World Wide Standardized Seismograph Network (WWSSN) in the early 1960s, only five earthquakes with body waves large enough to study teleseismically have occurred within or near the East Anatolian Fault Zone (Fig. 1). One of these (the Lice earthquake of 1975 September 6) has been studied already by Nábělek (1984). In this paper we examine the other four, using *P*- and *SH*-waveforms as well as first motion polarities to constrain their focal mechanisms. The resulting mechansims and slip vectors are much better constrained than those based on first motion polarities (McKenzie 1972; Jackson & McKenzie 1984) or *P*-waves (Eyidoğan 1983) alone.

2 EARTHQUAKE SOURCE MECHANISMS

2.1 Data reduction

We used both *P*- and *SH*-waveforms and first motion polarities of *P*-waves to constrain earthquake source parameters. The approach we followed is that described by

Molnar & Lyon-Caen (1989), which we also used in a study of earthquakes in the Hellenic Trench (Taymaz, Jackson & Westaway 1990) and in the North and Central Aegean Sea (Taymaz *et al.* 1991). We compared the shapes and amplitudes of long-period *P*- and *SH*-waveforms recorded by WWSSN stations in the distance range 30°–90° with synthetic waveforms. To determine source parameters we used McCaffrey & Abers's (1988) version of Nábělek's (1984) inversion procedure, which minimizes, in a weighted least-squares sense, the misfit between observed and synthetic seismograms (McCaffrey & Nábělek 1987; Nelson, McCaffrey & Molnar 1987; Fredrich, McCaffrey & Denham 1988). Seismograms are generated by combining direct (*P* or *S*) and reflected (*pP* and *sP*, or *sS*) phases from a point source embedded in a given velocity structure. Receiver structures are assumed to be homogeneous half-spaces. Amplitudes are adjusted for geometrical spreading, and for attenuation using Futterman's (1962) operator, with $t^* = 1$ s for *P* and $t^* = 4$ s for *SH*. As explained by Fredrich *et al.* (1988), uncertainties in t^* affect mainly source duration and seismic moment, rather than source orientation or centroid depth. Seismograms were weighted according to the azimuthal distribution of stations, such that stations clustered together were given smaller weights than those of isolated stations (McCaffrey & Abers 1988). The inversion routine then adjusts the strike, dip, rake, centroid depth and source time function, which is described by a series of overlapping isosceles triangles (Nábělek 1984) whose number and duration we selected.

Our experience with the inversion routine was similar to that of Nelson *et al.* (1987), McCaffrey (1988), Fredrich *et al.* (1988) and Molnar & Lyon-Caen (1989). For all except the Bingöl event (number 2 in Table 1) we found that a point source, in which all slip occurs at the same point (the centroid) in space but not in time, was a good approximation: i.e. we saw no indication of the systematic azimuthal variations in waveforms that might be associated with rupture propagation. Waveforms from the Bingöl event show evidence of multiple rupture, and we attempted to match them with a later subevent of a similar orientation to the first (see below for details). The focal sphere was generally covered by observations in all quadrants, though with more stations to the north than the south, and we found that estimates of the strike, dip, rake and centroid depth were relatively independent of each other. Thus if one parameter was fixed at a value within a few degrees or km of its value yielded by the minimum misfit of observed and synthetic seismograms, the inversion routine usually returned values for the other parameters that were close to those of the minimum misfit solution. The strikes and dips of nodal planes were consistent, within a few degrees, with virtually all first motion polarities (Fig. 2).

The estimate of seismic moment clearly depended on the duration of the source time function, and to some extent on centroid depth and velocity structure. As our main interest is in source orientation and depth, we did not concern ourselves much with uncertainties in seismic moment, which in most cases is probably about 30 per cent. We estimated the lengths of the time functions by increasing the number of isosceles triangles until the amplitudes of the later ones became insignificant. The seismogram lengths we selected for inversion were sufficient to include the reflected phases *pP*, *sP* and *sS*. We examined the *P*-waves for *PcP* arrivals, where they were anticipated within the selected window, but this phase was never of significant amplitude. *ScS* presented a greater problem, and we generally truncated our inversion window for *SH*-waves before the *ScS* arrival. Where *ScS* arrives within the window we retained, we have marked its arrival time explicitly (see, for example, BLA in Fig. 7).

All the events we analysed in Fig. 1 and Table 1 had centroid depths in the range 2–11 km. The source velocity structures we used to calculate the synthetic seismograms are listed in Table 2. Uncertainty in the average velocity above the source leads directly to an uncertainty in centroid depth, which we estimate to be about ±2 km.

2.2 Uncertainties in source parameters

Having found a set of acceptable source parameters, we followed the procedure described by McCaffrey & Nábělek (1987), Nelson *et al.* (1987), Fredrich *et al.* (1988), Molnar & Lyon-Caen (1989) and Taymaz *et al.* (1990, 1991), in which the inversion routine is used to carry out experiments to test how well individual source parameters are resolved. We investigated one parameter at a time by fixing it at a series of values either side of its value yielded by the minimum misfit solution, and allowing the other parameters to be found by the inversion routine. We then visually examined the quality of fit between observed and synthetic seismograms to see whether it had deteriorated from the minimum misfit solution. In this way we were able to estimate the uncertainty in strike, dip, rake and depth for each event. In common with the authors cited above, we believe this procedure gives a more realistic quantification of likely errors than the formal errors derived from the covariance matrix of the solution. We will now illustrate this procedure using the earthquake of 1971 May 22 (no. 2 in Table 1), near the city of Bingöl.

2.3 The Bingöl earthquake of 1971 May 22

The Bingöl earthquake was the most destructure in the East Anatolian Fault Zone since the installation of the WWSSN. Many cracks and en-échélon tension fissures were observed after the earthquake by Arpat & Şaroğlu (1972) and Seymen & Aydin (1972). The main ground rupture ran southwest through the town of Bingöl, where the maximum damage occurred. Tension cracks were oriented between 000° and 025°, in en-échélon patterns. Left-lateral shear zones were oriented 040° to 045°, and were traced for a distance of about 35 km (Seymen & Aydın 1972). The maximum lateral displacement was about 25 cm, with no significant vertical displacement.

The minimum misfit solution for the earthquake of 1971 May 22 is shown in Fig. 3. This solution is compatible with all first motion *P* polarities, shown in Fig. 2(b). The main rupture in this event had an almost pure strike–slip mechanism, consistent with left-lateral motion on a NE–SW striking fault plane, as seen in the surface rupture. This was the largest event in our study ($M_0 = 9.3 \times 10^{18}$ N m) and was well recorded at all azimuths. Many of the *P*-waveforms are complex, and varied in shape even between neighbouring stations on the focal sphere (see, for example, BUL and AAE, and NOR and GDH in Fig. 3).

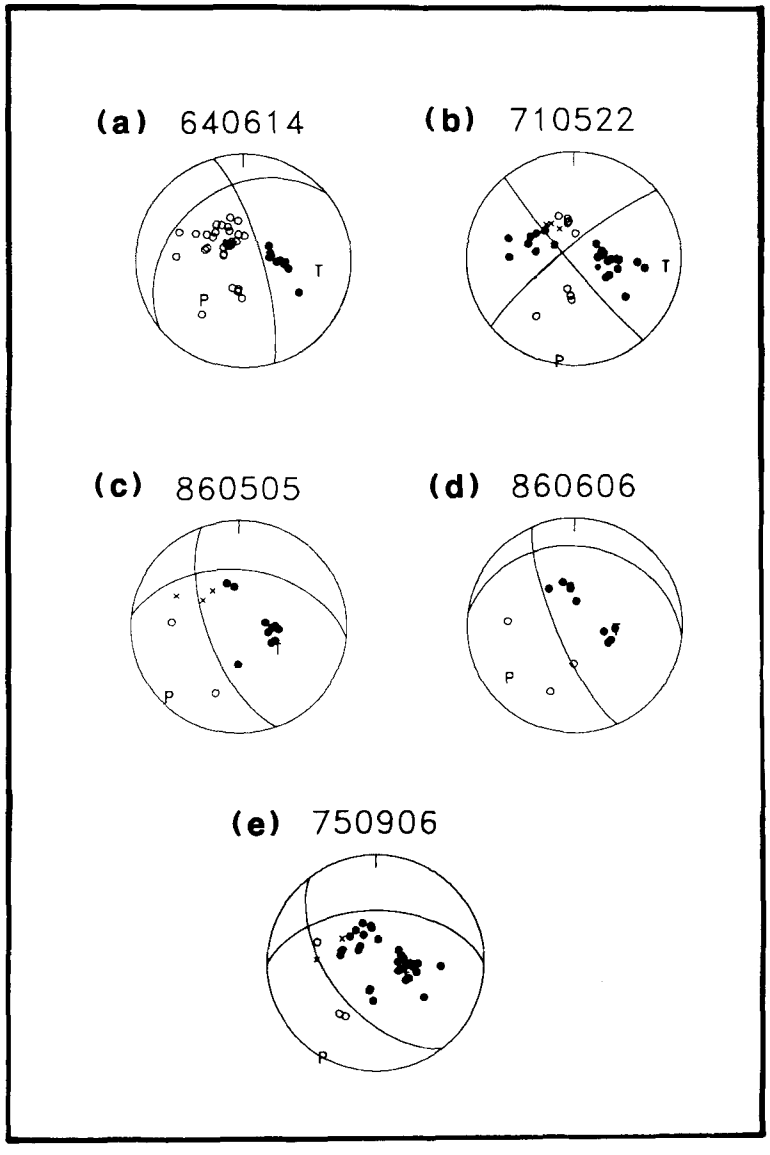

Figure 2. Lower hemisphere equal area projections of the first motion polarity data. Station positions of the focal sphere have been plotted using the same velocity below the source that was used in our waveform inversion procedure. Filled circles are compressional first motions, open are dilatational. All were read on long-period instruments of the WWSSN. Nodal planes are those of the minimum misfit solutions. Above each sphere is the event's date (year, month, day). Note that the apparent compressional reading in the dilatational quadrant of (a) is, in fact, a cluster of many dilatational readings from close stations.

The orientation of the source responsible for the early part of the seismograms is well constrained by first motion polarities (Fig. 2b) and by the change in polarities of *P*- and *SH*-waveforms across nodal planes (Fig. 3). There is a hint of a second subevent that might be responsible for the pulses observed 4–8 s after the *P* and *SH* arrivals at all azimuths. We were able to improve the fit of observed to synthetic waveforms by including a second subevent about 4 s after the first, with a similar mechansim (Fig. 3). We fixed the parameters of the first subevent and inverted for

Table 1. Source parameters of East Anatolian earthquakes obtained from body wave inversion.

No	Date (d m y)	Origin Time (h m s)	Location Lat. N(°)	Location Long. E(°)	m_b	M_s	M_o $\times 10^{16}$ (Nm)	Centr. Depth (km)	Strike (°)	Dip (°)	Rake (°)	Slip Vec. (°)
1	14.06.1964	121531.4	38.13	38.51	5.5	*5.7	63	11±2	227±5	29±5	−28 ± 10	072
2	22.05.1971	164359.8	38.89	40.52	5.9	*6.9	580	9±2	231±8	82 + 2/ − 5	3±10	051
	multiple	164403.6	38.85	40.42	—	—	350	6	232	71	16	—
†3	06.09.1975	092012.0	38.50	40.70	6.0	6.7	1000	5	270	50	50	052
4	05.05.1986	033538.0	38.02	37.79	5.7	*5.9	112	4±1	273±10	49±5	31±10	072
5	06.06.1986	103947.0	38.01	37.91	5.5	5.6	90	2±1	275±10	27±10	30±8	068

* After N. Ambraseys (pers. comm.).
† After J. Nábělek (1984).

Table 2. Source velocity structures used in waveform inversion.

Events (d m y)	V_p (kms^{-1})	V_s (kms^{-1})	Density (kgm^{-3})	Thickness (km)
14.06.1964	6.00	3.45	2780	6
22.05.1971	6.80	3.92	2910	half-space
05.05.1986	6.00	3.45	2780	half-space
06.06.1986				

those of the second subevent, including the separation in space and time between the two subevents. We found that including a second source with origin time 3.8 s after the first, and offset 17 km in the direction of 254°, produced synthetic waveforms that matched the observed waveforms better than the synthetics involving a single source alone: but the parameters of the second source are not well resolved. The fit between observed and synthetic waveforms is good, except for the amplitude of the *SH*-waveform at station MAT, which is close to the null axis in the radiation pattern and extremely sensitive to small perturbations. We could not improve its fit without severely worsening the fit at other stations. Figs 4 and 5 summarize some of the tests we carried out to estimate the uncertainties in strike, dip, rake and centroid depth. In Figs 4 and 5, the top row of waveforms compares observed *P* and *SH* seismograms (solid lines) at selected stations with synthetic seismograms (dashed lines) generated for the minimum misfit solution for the double shock. In Fig. 4, the second row shows the first subevent on its own. In row 3 of Fig. 4, we show waveforms from an inversion in which we fixed the strike, dip and rake to be that of Jackson & McKenzie's (1984) first motion solution, and allowed the depth, time function and moment to be free. The match of *P*-waveforms is not greatly inferior to that in the single shock inversion in row 2, but the match of *SH* at HKC and of *P* at GDH is certainly worse. To calculate the synthetic seismograms in rows 4 and 5 of Fig. 4, we fixed the centroid depth for the first subevent at values of 6 and 12 km, and allowed all the other parameters of the first subevent to change in the inversion, while the second subevent was held fixed at its minimum misfit solution. The fit of observed to synthetic seismograms is noticeable worse at stations marked by a vertical bar, as the pulse width narrows with decreasing depth and widens with increasing depth. Note that the fit at stations marked by an asterisk have improved: it is quite common for the fit at one or two stations to improve slightly when a parameter is set to a value that is clearly unacceptable because of a poor fit at many other stations (see also Molnar & Lyon Caen 1989). We found that changing the depth of the first subevent by more than 2 km produced a noticeable degradation in the fit of the waveforms, and we take this to be a realistic estimate of the uncertainty in focal depth. This estimate, which is listed in Table 1, does not include the uncertainty due to the unknown average velocity structure above the source.

Figure 5 shows similar tests to investigate the uncertainties in strike, dip and rake of the first subevent. The first row shows the minimum misfit solution with two subevents. In the following rows the second subevent was always held fixed to its minimum misfit solution while the individual parameters of first subevent were tested. Rows 2 and 3 illustrate tests for uncertainty in strike, which was fixed at 15° either side of the minimum misfit solution. The match of seismograms is noticeably worse, particularly for *SH* at HKC and BUL and for *P* at GDH. In rows 4 and 5 the dip has been fixed at values of 7° less and 3° more than that in row 1: this, too, degrades the fit of seismograms, particularly for *SH*. Finally, in rows 6 and 7, the rake has been fixed at 20° either side of the minimum misfit solution. Here, too, the degradation of the fit is clear, particularly for *SH*. In each of rows 2 and 7 one parameter has been perturbed from the minimum misfit solution and then fixed: yet the values returned by the inversion routine for the other parameters have not shifted significantly from those of the minimum misfit solution. This gives us some confidence that there is not significant trade-off between source parameters for this event. The greatest change occurs to the value of seismic moment, which varied by 20 per cent.

We carried out many experiments of the sort illustrated in Figs 4 and 5, and, based on these, estimate the source parameters and uncertainties for the first subevent of the 1971 May 22 Bingöl earthquake to be: strike $231 \pm 8°$; dip $82° + 2°/-5°$; rake $3° \pm 10°$, and depth 10 ± 2 km (though this does not include uncertainty related to velocity structure). Note that, for the tests in Fig. 5, we examined the uncertainty in strike of the auxiliary plane (striking NW–SE). The slip vector is perpendicular to this strike, and can thus be estimated as $051° \pm 8°$. Our tests for the second subevent showed that its source parameters are not as well resolved as those of the first: but it must be similar in orientation, and is probably offset about 17 km in a direction 254° from the first subevent.

2.4 The Malatya earthquake of 1964 June 14

Historical studies have shown that Malatya city and surroundings have been devasted by several major earthquakes in the past (Ergin, Güçlü & Uz 1967; Ambraseys 1989). The 1964 June 14 event was associated with minor ground features of uncertain tectonic origin (Barut & Gürel 1964). Some of the observed fissures were probably related to landsliding. First motion solutions for this event by McKenzie (1972), Canıtez & Üçer (1967), and Jackson & McKenzie (1984) are poorly constrained, but require a steep nodal plane striking NNW. Eyidoğan (1983) used long-period *P*-waveforms to estimate the depth, but the source orientation was not constrained tightly. We found 10 *P* and nine *SH* waveforms that were good enough to use within the inversion routine. The minimum misfit solution returned by the inversion procedure shows a normal fault mechanism with a large strike–slip component (Fig. 6); consistent with first motion polarities.

We carried out many experiments of the sort illustrated in Figs 4 and 5, and, based on these, estimate the source parameters and uncertainties of this event to be: strike $227° \pm 5°$; dip $29° \pm 5°$; rake $-28° \pm 10°$, and depth 11 ± 2 km.

2.5 The 1986 Doğanşehir earthquake sequences

Two damaging earthquakes on 1986 May 5 ($M_s = 5.8$) and 1986 June 6 ($M_s = 5.6$) occured on south of the town of Doğanşehir (marked D on Fig. 1). In this area, the East Anatolian Fault Zone meets the Bitlis Thrust Zone

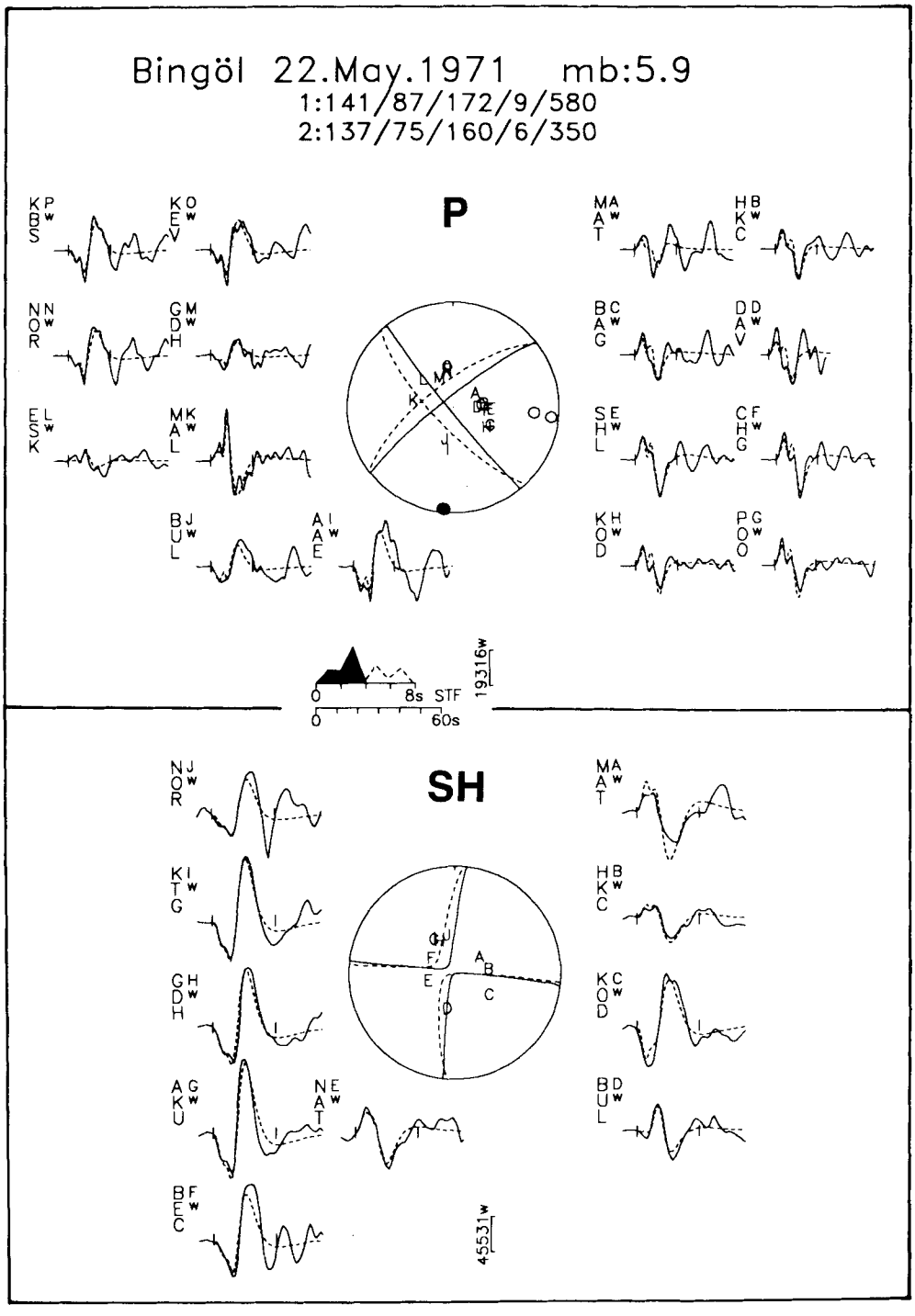

Figure 3. This (and subsequent similar figures) shows the radiation patterns and synthetic waveforms for the minimum misfit solution returned by the inversion procedure, as well as the observed waveforms. For the purposes of display, waveform amplitudes have been normalized to that of an instrument with a gain of 3000 at a distance of 40°. Solid lines are observed waveforms, and the inversion window is identified by vertical bars. Synthetic waveforms are dashed lines. The station code is identified to the left of each waveform, together with an upper case letter, which identifies its position on the focal sphere, and a lower case letter that indicates the type of instrument (w = WWSSN long period). The vertical bar beneath the focal sphere shows the scale in microns, with the lower case letter indicating the instrument type, as before. The source time function is shown in the middle of the figure, and beneath it is the time-scale used for the waveforms. Focal spheres are shown with *P* and *SH* nodal planes, in lower hemisphere projection. Station positions are indicated by letter, and are arranged alphabetically clockwise, starting from north. *P* and *T* axes are marked by solid and open circles. Beneath the header at the top of the figure, which shows the date and body wave magnitude, are five numbers which show the strike, dip, rake, centroid depth and seismic moment (in units of 10^{16} N m) of the minimum misfit solution. The nodal planes and time function of the postulated second subevent are shown by dashed lines. The strike, dip, rake, depth and moment of the second subevent are shown below those of the first in the heading.

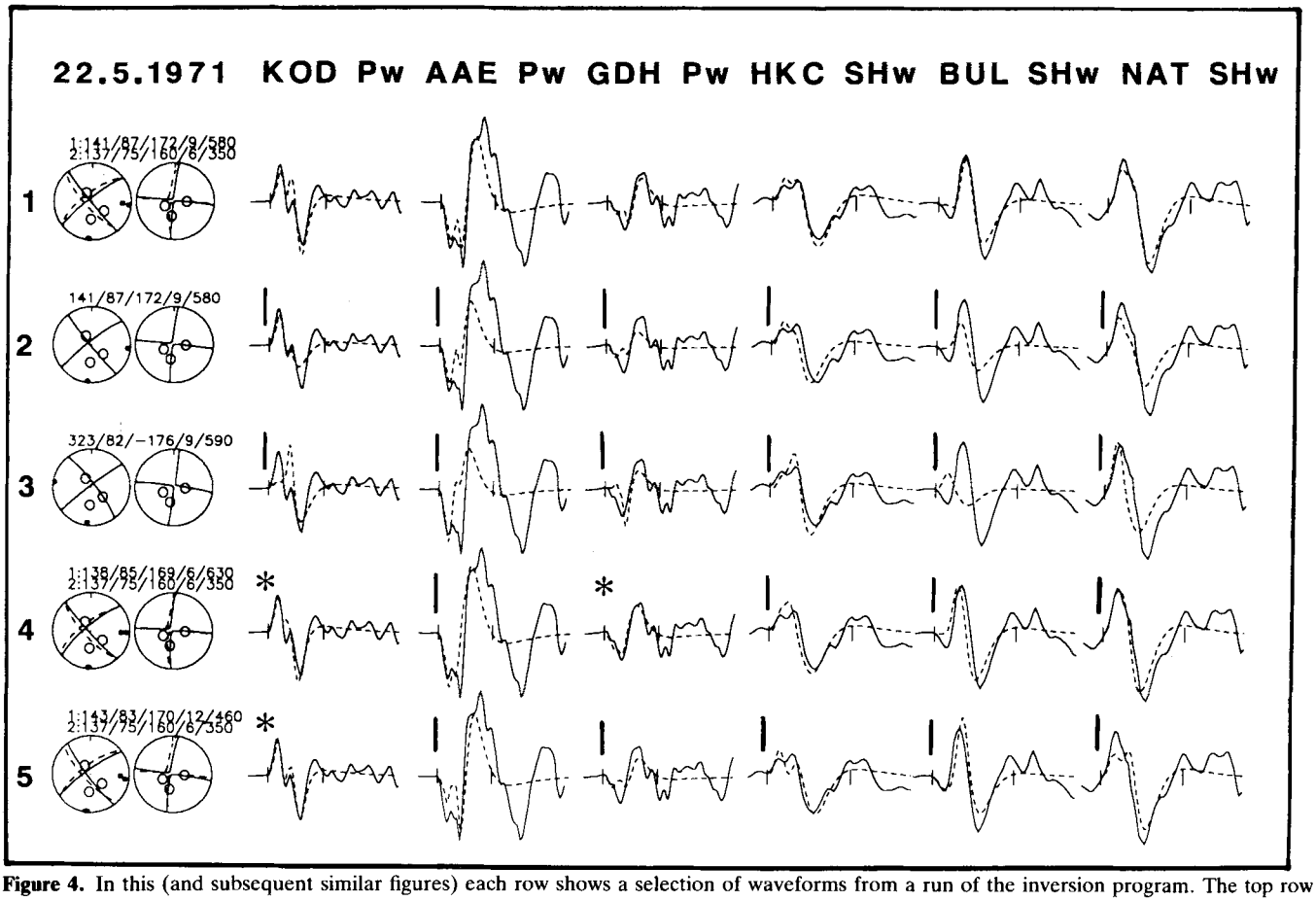

Figure 4. In this (and subsequent similar figures) each row shows a selection of waveforms from a run of the inversion program. The top row always shows waveforms from the minimum misfit solution. The stations are identified at the top of each column, with the type of waveform marked by *P* or *SH* and followed by the instrument type, as in Fig. 3. At the start of each row are the *P* and *SH* focal spheres for the focal parameters represented by the five numbers (strike, dip, rake, depth and moment, as in Fig. 3), showing the positions on the focal spheres of the stations chosen. The displayed waveforms are in the same convention as in Fig. 3, but in this type of figure the large bars show matches of observed to synthetic waveforms that are worse than in the minimum misfit solution, and asterisks show matches that are improvements. The second row is the first subevent on its own. In the third row the strike, dip and rake were fixed to the values of Jackson & McKenzie's (1984) first motion solution, while the other parameters were left free. In rows 4–5 the depth has been held fixed at values of 6 and 12 km, while the other parameters were left free.

(Perinçek & Çemen 1990), and separates into segments and bends which may be sites of higher convergent strain (Şengör *et al.* 1985). The Sürgü fault, which is one of the prominent tectonic features in this region, is a left-lateral strike–slip fault (Arpat & Şaroğlu 1975) that is located very close to the epicentres of both Doğanşehir events. The strike of the shallow dipping nodal planes returned by the inversion routine, their epicentral locations, and other field observations imply that the Sürgü fault may have been associated with these events (Fig. 1).

2.6 The Doğanşehir earthquake of 1986 May 5

The waveforms for this event are shown in Fig. 7. Its mechanism is well constrained, particularly by the *SH*-waves, and is consistent with first motion polarities (Fig. 2c). The azimuthal coverage of the focal sphere is good for both *P*- and *SH*-waveforms and there is excellent coherence between waveforms from adjacent stations on the focal sphere. We could not model the large amplitudes observed in the later part of some *SH*-waveforms (mainly at southern stations), which might be associated with rupture propagation or structural effects (Fig. 7).

Based on experiments of the type illustrated in Figs 4 and 5 our estimate of the source orientation in this event is: strike 273° ± 10°; dip 49° ± 5°; rake 31° ± 10° and depth 4 ± 1 km.

In Fig. 8(a), we compare our minimum misfit solution with waveforms from an inversion in which we fixed the strike, dip and rake to be that of CMT solution published at PDE monthly listings by USGS and allowed the depth, time function and moment to be free. The CMT solution differs from our solution by 2° in strike, 15° in dip and 9° in rake. The difference in dip is marginally outside the acceptable errors in our solution (Table 1), and their solution produces a worse fit to the *P*-waves at NAI and KEV.

2.7 The Doğanşehir earthquake of 1986 June 6

This was the second largest event of the sequence, occuring about a month after the main shock. The minimum misfit solution is shown in Fig. 9, and first motion polarities in Fig. 2(d). The epicentre of the 1986 June 6 event is located approximately 10 km NE of the main shock, causing some

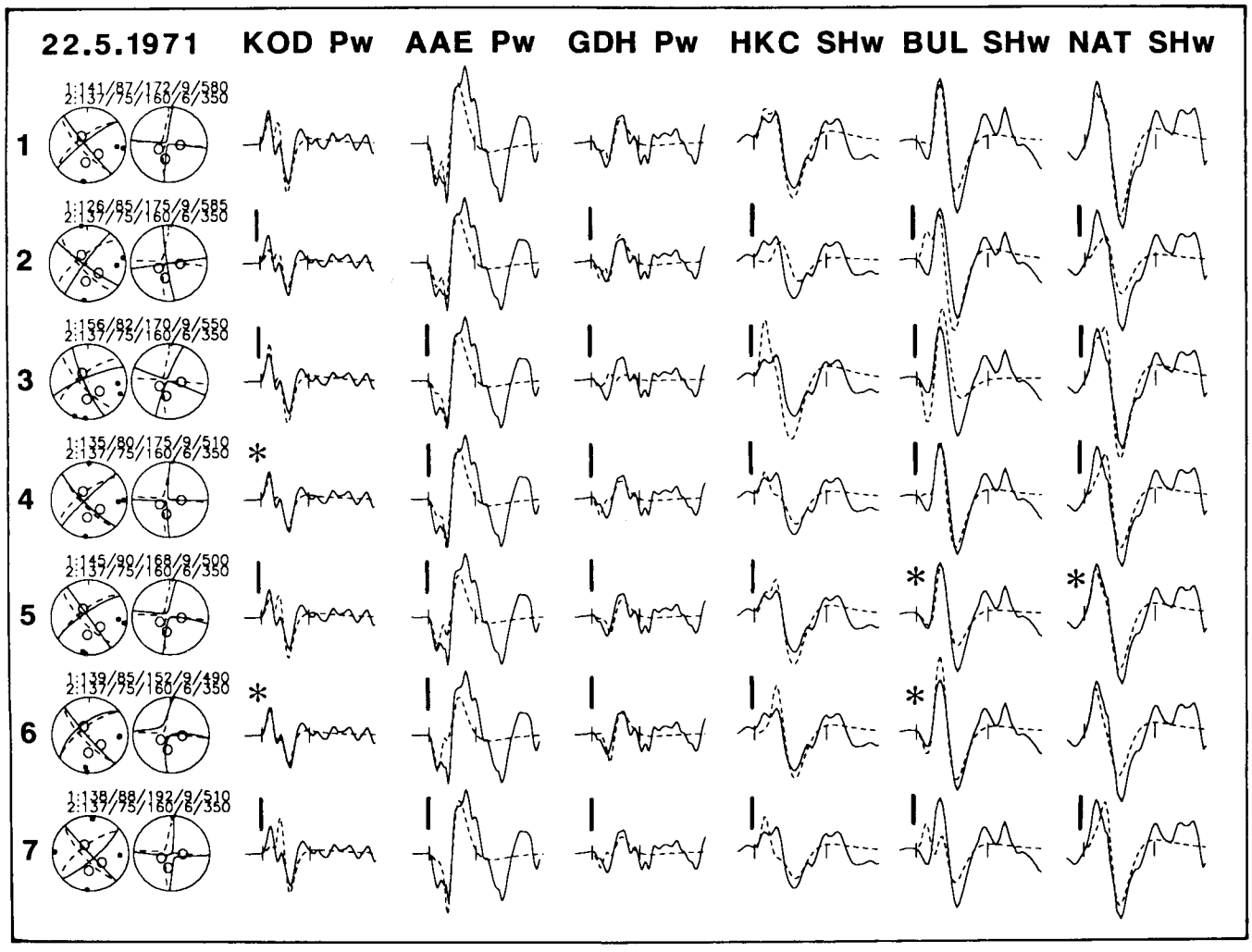

Figure 5. This figure follows the convention of Fig. 4. The top row is the minimum misfit solution with two subevents. The parameters of the second subevent are held fixed in rows 2–7. In rows 2–3 the strike of the first subevent has been held fixed at values of 126° and 156°; in rows 4–5 the dip has been held fixed at values of 80° and 90° and finally in rows 6–7 the rake has been held fixed at values of 152° and 192°, while the other parameters have been left free.

additional damage to houses which were slightly effected from first shock. Once again, we could not reproduce the large amplitudes observed in the later part of some *SH*-waveforms (mainly at southern stations).

In Fig. 8(b), we compare our minimum misfit solution (top row) with the CMT solution given in the PDE monthly listings by USGS, and inverted for depth and source time function. The CMT solution differs from our solution by 2° in strike, 13° in dip and 66° in rake. The fit of waveforms is noticeably worse than in the minimum misfit solution, with the wrong polarity for the *P*-wave at KEV, and worse fits to the *SH*-waves at BUL and KBS. In addition, the CMT solution is not compatible with first motions at stations to the north. Based on experiments similar to those in Figs 4 and 5, we estimate the source orientation to be strike 275° ± 10°; dip 27° ± 10°; rake 30° ± 8°; and centroid depth 2 ± 1 km.

2.8 The Lice earthquake of 1975 September 6

The *P*- and *SH*-waveforms of this earthquake were studied by Nábělek (1984) using essentially the same program and technique as we used for the events we studied. His minimum misfit solution is expected to be better constrained than the first motion solution of Jackson & McKenzie (1984), with which it is compatible (Fig. 2e), and we have not repeated his work.

The earthquake was associated with thrust faulting at the surface, dipping north, with a length of about 20 km along strike (Arpat 1977). The slip vector in this event is thus directed NE, and may be related to the Arabia–Turkey motion, rather than the Arabia–Eurasia motion (which should be NNW–SSE), as implied by Jackson & McKenzie (1984). We therefore include the Lice earthquake in our discussion of the tectonics, in the next section.

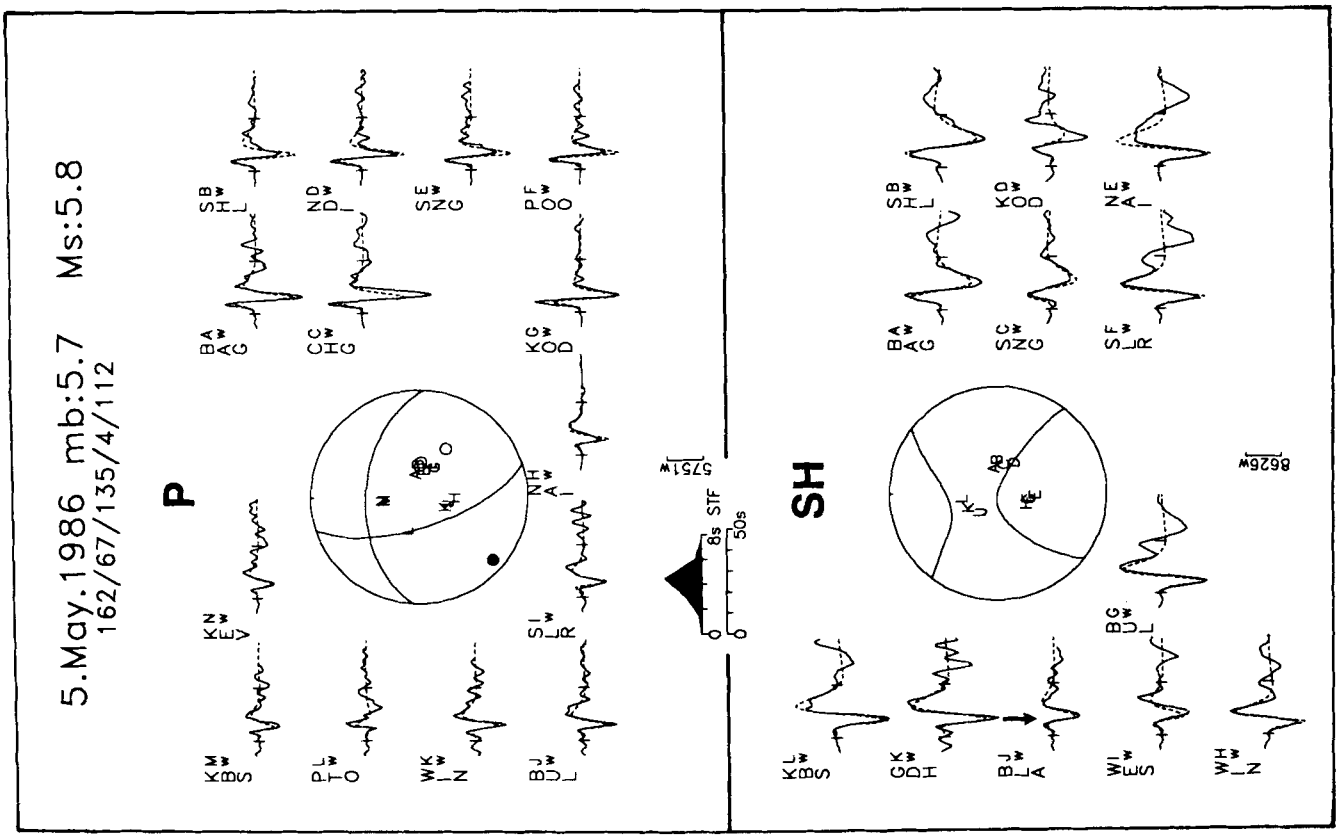

Figure 7. Minimum misfit solution for the earthquake of Doğanşehir 1986 May 5. The display convention is the same as in Fig. 3.

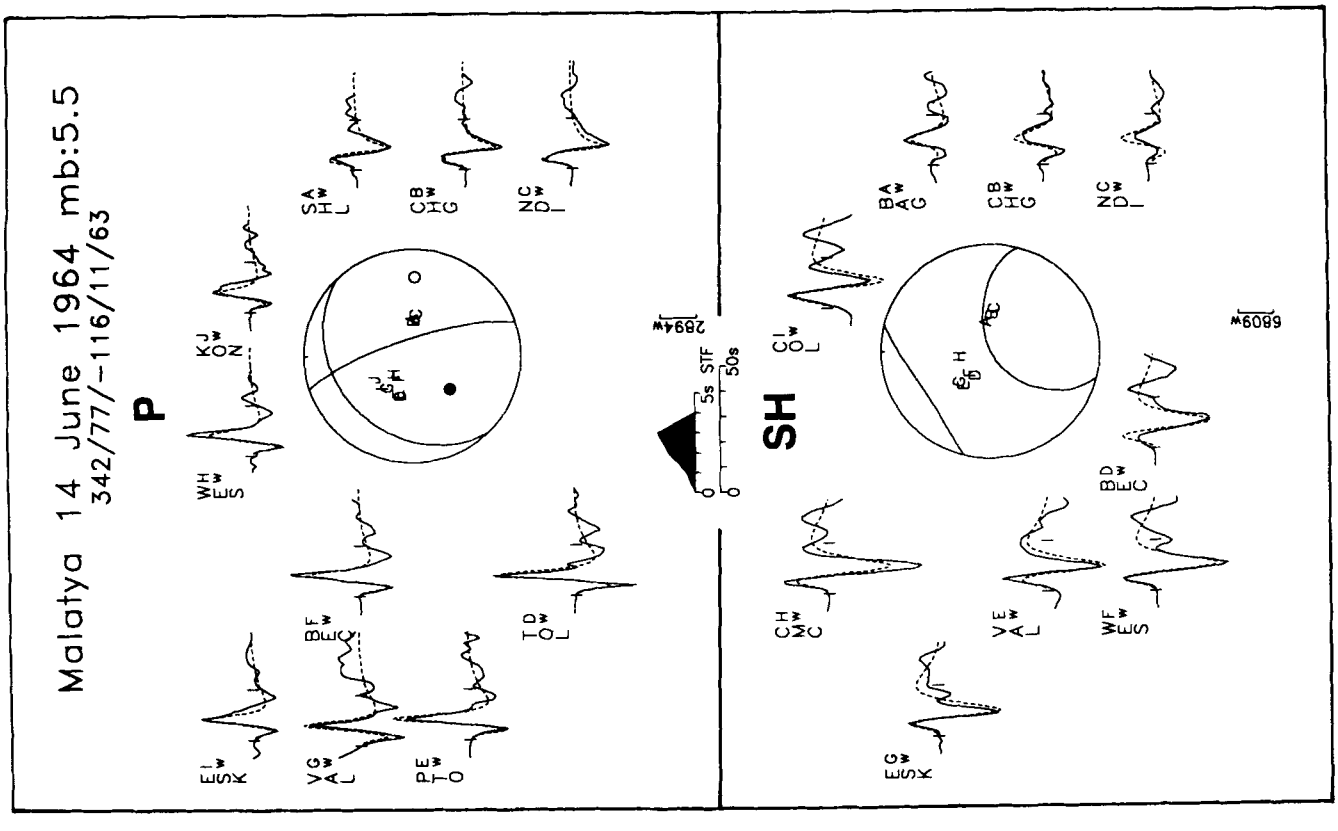

Figure 6. Minimum misfit solution for the earthquake of Malatya 1964 June 14. The display convention is the same as in Fig. 3.

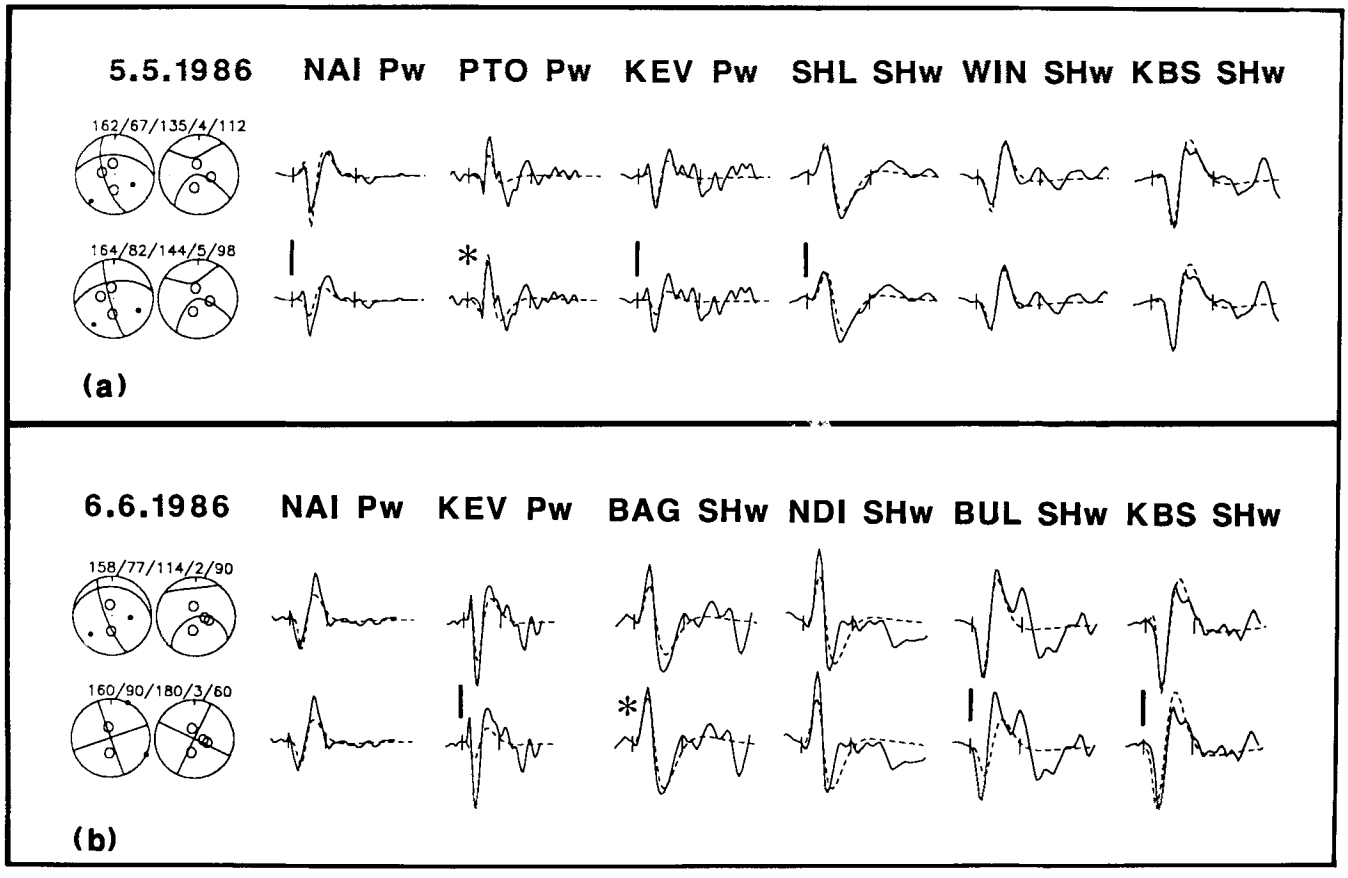

Figure 8. In this figure we compare selected waveforms from misfit solutions for the two Doğanşehir events with those generated by sources with the orientations of the CMT solutions reported in the PDE. The format of the figure is that of Fig. 4. (a) The event of 1986 May 5. Waveforms for the minimum misfit solution are shown in the top row. In the second row the strike, dip and rake were fixed to the values of the CMT solution, while the depth and source time function were left free. (b) The event of 1986 June 6. The minimum misfit solution is in the top row and the CMT solution in the second row, as in (a).

3 DISCUSSION

Figure 10 shows the directions of the horizontal projections of the slip vectors (marked as boldfaced arrows) in the earthquakes in Fig. 1 and Table 1. To compile Fig. 10 we have had to identify the fault plane from the two possible nodal planes in each fault plane solution. Some of the earthquakes were associated with surface faulting, and the choice of nodal plane was thus straightforward. These events were numbers 2 (Seymen & Aydın 1972) and 3 (Arpat 1977; Nábělek 1984) in Table 1. The choice of nodal plane in events 1, 4 and 5 is difficult, because there are no reported observations of faulting in the field. We have assumed that the steep NNW striking nodal planes are the auxiliary planes, and that the shallow dipping, NE–SW striking nodal planes are the fault planes. This choice is consistent with oblique left-lateral and reverse faulting on the E–W Sürgü fault in the two Doğanşehir events. There are no major faults with a NNW strike in the region, and motion on the steep NNW-strike nodal planes might be expected to produce surface faulting (which was not observed), given the very shallow centroid depths of events 4 and 5 (Table 1). We are thus reasonably confident that we have identified the fault planes correctly in events 1, 4 and 5.

If we are correct in our identification of the fault planes in events 1, 4 and 5, then the four events we studied, and the Lice event of 1975 September 6, all have remarkably similar slip vectors (Table 1 and Fig. 10). The mean slip vector direction is $063° \pm 10°$. This direction is very close to the 060° direction assumed for the Arabia–Turkey motion by Jackson & McKenzie (1984). It is possible that these earthquake slip vectors represent the direction of motion between Arabia and Turkey. If they do, then this direction may be used to complete the velocity triangle between Arabia, Turkey and Eurasia (Fig. 11). The slip rate on the North Anatolian Fault Zone is then estimated to be $38\ \text{mm yr}^{-1}$, with a range of 31 to $48\ \text{mm yr}^{-1}$. The overall slip rate on the East Anatolian Fault Zone would then be $29\ \text{mm yr}^{-1}$, with a range of 25 to $35\ \text{mm yr}^{-1}$. These values differ a little from the slip rates on the North and East Anatolian Fault Zones estimated by Jackson & McKenzie (1984, 1988a), who obtained values of 30 and $34\ \text{mm yr}^{-1}$ respectively, because they used the Arabia–Eurasia pole and rate of Chase (1978), rather than the more recent NUVEL-1 plate model of DeMets *et al.* (1990). The revised poles and rates of rotation for the Arabia–Turkey–Eurasia motions are given in Table 4.

It is clear from the mechanisms and locations of the

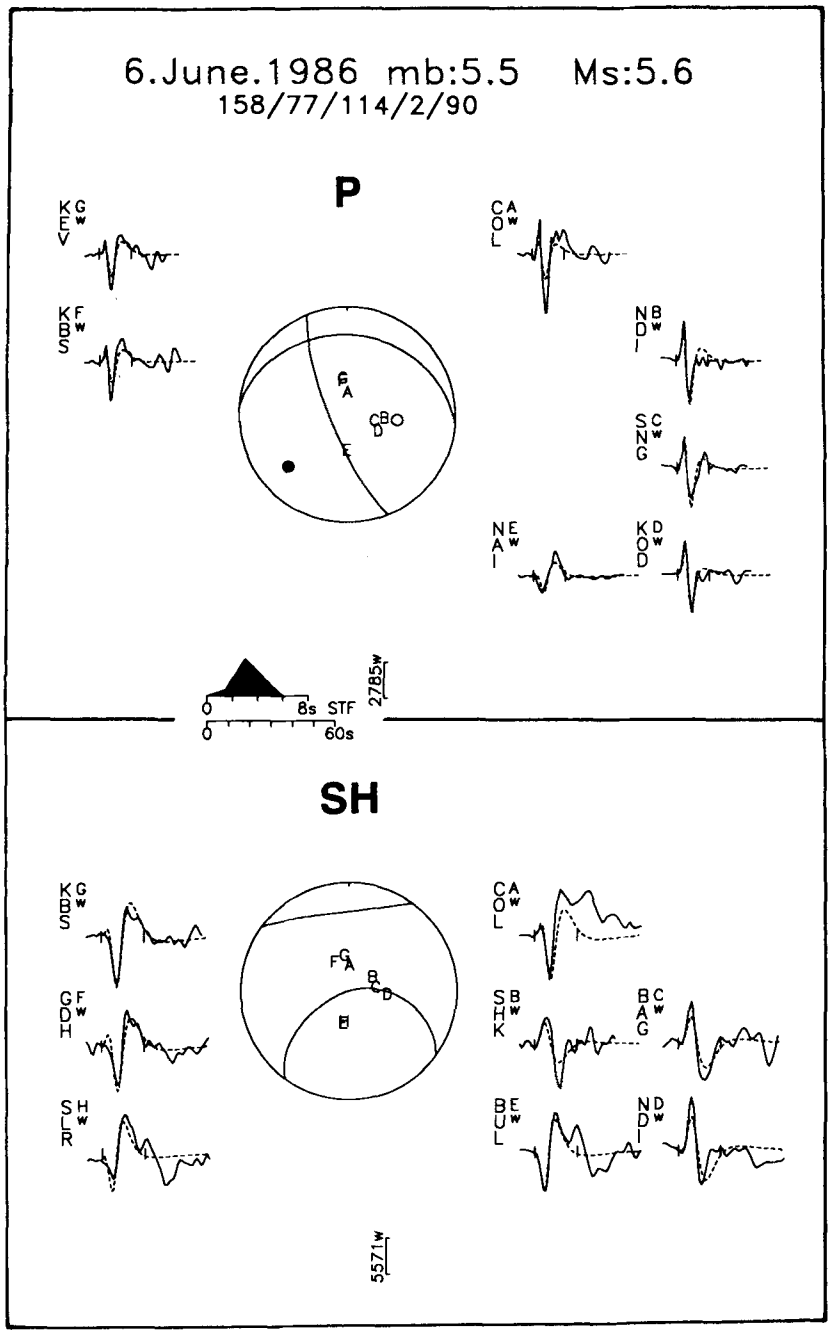

Figure 9. Minimum misfit solution for the earthquake of Doğanşehir 1986 June 6. The display convention is the same as in Fig. 3.

events we studied that they did not all occur on a single left-lateral, NE–SW striking strike–slip fault. The present and historical seismicity within the East Anatolian Fault Zone is distributed over a zone of perhaps 100 km width. For this reason we must be cautious in assuming that the slip vectors represent the direction of overall motion across the zone: once deformation is distributed, rotations about a vertical axis are possible, and the slip vectors on the faults within the zone may differ from the overall motion across it (McKenzie & Jackson 1983; Jackson & McKenzie 1988a). we are unaware of any palaeomagnetic evidence concerning possible rotations in the East Anatolian Fault Zone, and because the zone is much narrower than the very diffuse bands of deformation in the Aegean region or in Iran it may be that such rotations have not occurred.

One of the remarkable features of the events we studied in the East Anatolian Fault Zone was the variety of the focal mechanisms, including oblique normal and reverse faulting, in contrast to the simple strike–slip solutions on the North Anatolian Fault (see Jackson & McKenzie 1984). If the present-day Arabia–Turkey–Eurasia relative motions may be represented by the simple velocity triangle in Fig. 11, the geometry is only stable if the Arabia–Eurasia motion is taken up on a boundary with the same strike as the North

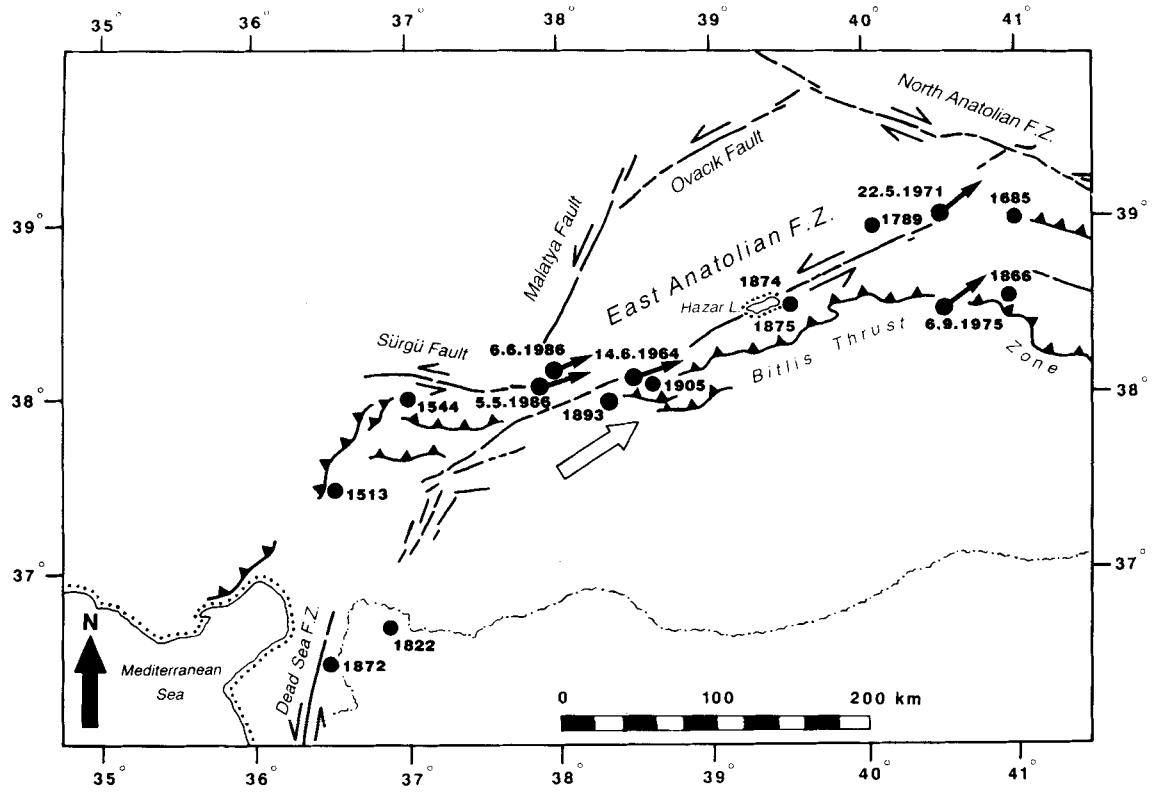

Figure 10. Horizontal projections of the slip vectors for the focal mechanisms obtained by our inversion procedure. Dates identify the events in Fig. 1 and Table 1. Also shown are the approximate locations of historical events that are summarized in Table 3 (from Ambraseys 1989). The large open arrow shows the direction of relative motion between Arabia and Turkey assumed by Jackson & McKenzie (1984).

Anatolian Fault. There is some indication that this is so: the 1966 Varto earthquakes occurred on an apparent continuation of the North Anatolian Fault SE of Karliova, with reverse and right-lateral strike–slip motion in a direction similar to that of the Arabia–Eurasia motion predicted by NUVEL-1 (see Ambraseys & Zatopek 1968; Jackson & McKenzie 1984). The 'triple-junction' would then migrate west relative to Eurasia with the same velocity as the slip rate on the North Anatolian Fault, and the SE end of North Anatolian Fault would change its sense of motion from pure strike–slip to reverse and right-lateral motion, as seen in the Varto earthquakes. However, some of the Arabia–Eurasia motion is clearly taken up north of Varto, towards the

Table 3. Large earthquakes ($M_s = 6.6$) in or near the EAF Zone 1500–1988. Modified from Ambraseys (1989).

Date (y m d)	Time (h m)	Epicentre N(°)	Epicentre E(°)	Q	M_s	Geographical Location
1513	—	37.5	36.5	B	7.4+	Tarsus-Malatya
1544 Apr 22	—	38.0	37.0	B	6.7+	Zitun-Malatya
1685 Nov 22	2300	39.0	41.0	B	6.7	Gönek
1789 May 29	—	39.0	40.0	B	7.0+	Palu
1822 Aug 13	2040	36.7	36.9	A	7.4+	Aafrine
1866 June 20	1400	38.5	40.9	A	6.8–	Kulp
1872 Apr 3	0740	36.4	36.5	A	7.2–	Amik Gölü
1874 May 3	0700	38.5	39.5	A	7.1+	Gölcük Gölü I
1875 Mar 3	2248	38.5	39.5	A	6.7	Gölcük Gölü II
1893 Mar 2	2251	38.0	38.3	A	7.1+	South Malatya
1905 Dec 4	0704	38.1	38.6	A	6.8*	Malatya

Q = estimated location accuracy, A= 10-40 km; B= 50-90 km.
M_s= estimated surface-wave magnitude from felt effects. Plus/minus signs indicate estimates probably underestimated/overestimated respectively. Asterisked value is from teleseismic data.

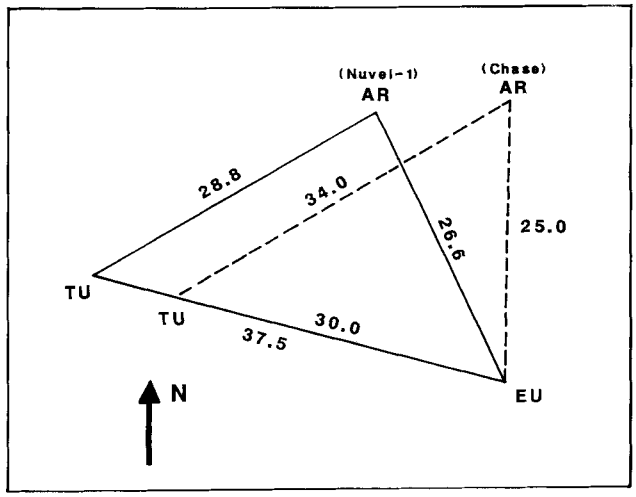

Figure 11. Velocity triangle for East Anatolia. AR = Arabia, EU = Eurasia, TU = Turkey. The dashed lines assume the Arabia–Eurasia pole and rotation rate from Chase (1978), as used by Jackson & McKenzie (1984). The solid lines are the Arabia–Eurasia motion from NUVEL-1 (DeMets *et al.* 1990). The direction of the Turkey–Arabia motion is taken as 240° and the direction of the Turkey–Eurasia motion is from the pole obtained by Jackson & McKenzie (1984).

Table 4. Revised Euler poles for Turkey–Arabia–Eurasia motion.

Euler poles	Lat.	Long.	Rate ($\times 10^{-7}$ °/yr)
Arabia-Eurasia†	24.6	13.7	5.20
Turkey-Eurasia	14.6	34.0	7.78
Turkey-Arabia	−3.3	61.9	3.51

† from NUVEL-1 (DeMets et al., 1990).

Caucasus, and this interpretation may be too simplistic. If the Arabia–Eurasia motion just east of Karlıova is not taken up in this simple fashion, the geometry is not stable, and must change. The complexity of the focal mechanisms and structure in the East Anatolian Fault Zone compared with the North Anatolian Fault Zone suggest that it is the East Anatolian Fault Zone that is the less-developed, and may be changing to accommodate any instability of the kinematics.

If the slip across the East Anatolian Fault Zone really is in the range 25–35 mm yr^{-1}, it is of interest to know whether there are sufficient earthquakes to account for this motion. If we take all the large earthquakes reported in or near the zone by Ambraseys (1989), given in Table 3, and include the two largest in our study (numbers 2 and 3 in Table 1), we can estimate their total contribution to the seismic moment release. Using Ekström & Dziewonski's (1988) global M_s:M_0 relation, and assuming an error of ±0.3 units in each magnitude determination, we obtain a moment rate of 16.1×10^{17} N m yr^{-1}, with a range of 5.8 to 45.1×10^{17} N m yr^{-1}. If all these events involve left-lateral slip on a NE striking fault (which must be unlikely, given their locations and probable mechanisms) this moment rate could account for 7.2 mm yr^{-1} of slip on a fault 500 km long extending to 15 km depth, with a range of 2.6 to 20.0 mm yr^{-1}. The inclusion of smaller earthquakes will increase this slip estimate by perhaps 50 per cent (Molnar 1979). The assumption of the source mechanisms being all NE-striking strike–slip faults means that these estimates are probably too high, but given the range of mechanisms in Fig. 1 it is probably not worth attempting more sophisticated calculations. We conclude that a significant fraction of the slip across the East Anatolian Fault Zone is likely to be accommodated seismically, but whether there is a substantial contribution from aseismic deformation processes, as, for example, in SW Iran and the Hellenic Trench (Jackson & McKenzie 1988a), is less certain.

ACKNOWLEDGMENTS

This research would not have been done without the help of R. McCaffrey and G. Abers, whose program and guidance were essential. Doğan Perinçek generously made available some unpublished tectonic maps, which are used to compile Fig. 1. We thank N. Lybéris for a preprint of his work, and Dan McKenzie and an anonymous reviewer for helpful suggestions. This work was supported by the Turkish Ministry of Higher Education and NERC. HE thanks the Royal Society and TÜBİTAK for supporting him at the initial stage of this study. JJ thanks the Dean of the School of Earth Sciences, Stanford University, for supporting him during the completion of this work. Cambridge Earth Sciences contribution no. 1786.

REFERENCES

Ambraseys, N. N., 1970. Some characteristic features of the North Anatolian Fault Zone, *Tectonophysics*, **9**, 143–165.

Ambraseys, N. N., 1971. On the value of historical records of earthquakes, *Nature*, **232**, 375.

Ambraseys, N. N., 1989. Temporary seismic quiescence: SE Turkey, *Geophys. J. Int.*, **96**, 311–331.

Ambraseys, N. N. & Zatopek, A., 1968. The Varton, Üstükıran (Anatolia) earthquake of 1966 August 19: a summary of a field report, *Bull. seism. Soc. Am.*, **58**, 47–102.

Arpat, E., 1977. 1975 Lice Depremi, *Yeryuvarı ve İnsan*, **2**, 15–28.

Arpat, E. & Şaroğlu, F., 1972. The East Anatolian Fault system: thoughts on its development, *Bull. Miner. Res. Explor. Inst., Turkey*, **78**, 33–39.

Arpat, E. & Şaroğlu, F., 1975. Türkiye'deki bazı önemli genç tektonik olaylar (On some important young tectonic events in Turkey), *Türkiye Jeoloji Kurumu Bülteni*, **18**, 29–41.

Barka, A. A. & Kadinsky-Cade, K., 1988. Strike-slip fault geometry in Turkey and its influence on Earthquake activity, *Tectonics*, **7**, 663–684.

Barut, Z. & Gürel, O., 1964. 14.06.1964 Malatya Depremi Rap. T. C. Bayındırlık ve İskan Bakanlığı, *Deprem Araştırma Enstitüsü Müd.* (in Turkish).

Canıtez, N. & Üçer, B., 1967. Computer determinations for the fault plane solutions in and near Anatolia, *Tectonophysics*, **4**, 235–244.

Chase, C. G., 1978. Plate kinematics: the Americas, East Africa, and the rest of the world, *Earth planet. Sci. Lett.*, **37**, 355–368.

DeMets, C., Gordon, R. G., Argus, D. F. & Stein, S., 1990. Current plate motions, *Geophys. J. Int.*, **101**, 425–478.

Dewey, J. F., Hempton, M. R., Kidd, W. S. F., Şaroğlu, F. & Şengör, A. M. C., 1986. Shortening of continental lithosphere: the neotectonics of Eastern Anatolia: a young collision zone, in *Collision Tectonics*, vol. 19, pp. 3–36, eds Coward, M. P. & Ries, A. C., Spec. Publ. Geol. Soc. London, Blackwell Scientific Publications, Oxford.

Ekström, G. & Dziewonski, A. M., 1988. Evidence of bias in the estimation of earthquake size, *Nature*, **332**, 319–323.

Ergin, K., Güçlü, U. & Uz, Z., 1967. A catalogue of earthquakes of Turkey and surrounding areas (11 A.D. to 1964 A.D.), *İTÜ Maden Fak. Arz Fiziği Yayın.*, no. 28, İstanbul.

Eyidoğan, H., 1983. Bitlis-Zağros Bindirme Kuşağının Sismotektonik Özellikleri, *PhD thesis*, İTÜ Maden Fakültesi, İstanbul.

Fredrich, J., McCaffrey, R. & Denham, D., 1988. Source parameters of seven large Australian earthquakes determined by body waveform inversion, *Geophys. J.*, **95**, 1–13.

Futterman, W. I., 1962. Dispersive body waves, *J. geophys. Res.*, **67**, 5 279–5 291.

Jackson, J. A. & McKenzie, D., 1984. Active tectonics of the Alpine–Himalayan Belt between western Turkey and Pakistan, *Geophys. J. R. astr. Soc.*, **77**, 185–264.

Jackson, J. A. & McKenzie, D., 1988a. The relationship between plate motions and seismic moment tensors, and the rates of active deformation in the Mediterranean and the Middle East, *Geophys. J. Int.*, **93**, 45–73.

Jackson, J. A. & McKenzie, D., 1988b. Rates of active deformation in the Aegean Sea and surrounding areas, *Basin Res.*, **1**, 121–128.

Lybéris, N., Yürür, T., Chorowicz, J., Kasapoğlu, E. & Gündoğdu, N., 1990. The East Anatolian Fault: An oblique collisional belt, *Tectonophysics*, in press.

McCaffrey, R., 1988. Active tectonics of the Eastern Sunda and Banda Arcs, *J. geophys. Res.*, **93**, 15 163–15 182.

McCaffrey, R. & Nábělek, J., 1987. Earthquakes, gravity, and the

origin of the Bali Basin: an example of a nascent continental fold-and-thurst belt, *J. geophys. Res.*, **92,** 441–460.

McCaffrey, R. & Abers, G., 1988. SYN3: A program for inversion of teleseismic body wave forms on microcomputers, *Air Force Geophysics Laboratory Technical Report,* AFGL-TR-88-0099, Hanscomb Air Force Base, MA.

McKenzie, D., 1972. Active tectonics of the Mediterranean Region, *Geophys. J. R. astr. Soc.*, **30,** 109–185.

McKenzie, D., 1976. The East Anatolian Fault: A major structure in eastern Turkey, *Earth planet. Sci. Lett.*, **29,** 189–193.

McKenzie, D. & Jackson, J. A., 1983. The relationship between strain rates, crustal thickening paleomagnetism, finite strain and fault movements within a deforming zone, *Earth planet. Sci. Lett.*, **65,** 182–202.

Molnar, P., 1979. Earthquake recurrence intervals and plate tectonics, *Bull seism. Soc. Am.*, **69,** 115–133.

Molnar, P. & Lyon-Caen, H., 1989. Fault plane solutions of earthquakes and active tectonics of the Tibetan Plateau and its martins, *Geophys. J. Int.*, **99,** 123–153.

Nábělek, J. L., 1984. Determination of earthquake source parameters from inversion of body waves, *PhD thesis*, MIT, Cambridge, MA.

Nelson, M. R., McCaffrey, R. & Molnar, P., 1987. Source parameters for 11 earthquakes in the Tien Shan, Central Asia, determined by *P* and *SH* waveform inversion, *J. geophys. Res.*, **92,** 12 628–12 648.

Perinçek, D., 1979. Geological investigation of the Çelikhan–Sincik–Koçali area (Adıyaman Province), *İst. Ün. Fen. Fak. Mec.*, B, **44,** 127–147.

Perinçek, D. & Çemen, İ., 1990. The structural relationship between the East Anatolian and Dead Sea fault zones in southeastern Turkey, *Tectonophysics*, **172,** 331–340.

Perinçek, D., Günay, Y. & Kozlu, H., 1987. New observations on strike–slip faults in east and southeast Anatolia, *7th Biannual Petroleum Congress of Turkey*, pp. 89–103, Ankara.

Philip, H., Cisternas, A., Gvishiani, A. & Gorshkov, A., 1989. The Caucasus: an actual example of the initial stages of continental collision, *Tectonophysics*, **161,** 1–12.

Şengör, A. M. C., Görür, N. & Şaroğlu, F., 1985. Strike slip faulting and related basin formation in zones of tectonic escape: Turkey as a case study, in *Strike Slip Deformation, Basin Formation, and Sedimentation,* No. 37, pp. 227–264, Society of Economic Paleontologists and Mineralogists, Tulsa, OK.

Seymen, İ. & Aydın, A., 1972. The Bingöl earthquake fault and its relation to the North Anatolian Fault zone, *Bull. Miner. Res. Explor. Inst., Turkey*, **79,** 1–8.

Taymaz, T., Jackson, J. A. & Westaway, R., 1990. Earthquake mechanisms in the Hellenic Trench near Crete, *Geophys. J. Int.*, **102,** 695–731.

Taymaz, T., Jackson, J. A. & McKenzie, D., 1991. Active tectonics of the north and central Aegean Sea, *Geophys. J. Int.*, **106,** 433–490.